

---

# Alleviating Exposure Bias in Diffusion Models through Sampling with Shifted Time Steps

---

Mingxiao Li\*, Tingyu Qu\*, Wei Sun & Marie-Francine Moens

Department of Computer Science, KU Leuven

{mingxiao.li,tingyu.qu,wei.sun,sien.moens}@kuleuven.be

## Abstract

Denoising Diffusion Probabilistic Models (DDPM) have shown remarkable efficacy in the synthesis of high-quality images. However, their inference process characteristically requires numerous, potentially hundreds, of iterative steps, which could lead to the problem of exposure bias due to the accumulation of prediction errors over iterations. Previous work has attempted to mitigate this issue by perturbing inputs during training, which consequently mandates the retraining of the DDPM. In this work, we conduct a systematic study of exposure bias in diffusion models and, intriguingly, we find that the exposure bias could be alleviated with a new sampling method, without retraining the model. We empirically and theoretically show that, during inference, for each backward time step  $t$  and corresponding state  $\hat{x}_t$ , there might exist another time step  $t_s$  which exhibits superior coupling with  $\hat{x}_t$ . Based on this finding, we introduce an inference method named Time-Shift Sampler. Our framework can be seamlessly integrated with existing sampling algorithms, such as DDIM or DDPM, inducing merely minimal additional computations. Experimental results show that our proposed framework can effectively enhance the quality of images generated by existing sampling algorithms.

## 1 Introduction

Denoising Diffusion Probabilistic Models (DDPM) (Ho et al., 2020; Sohl-Dickstein et al., 2015) are a class of generative models that has shown great potential in generating high-quality images. (Dhariwal and Nichol, 2021; Ramesh et al., 2022; Rombach et al., 2022a; Nichol et al., 2022). DDPM consists of a forward and a reverse backward process. In the forward process, images are progressively corrupted with Gaussian noise in a series of time steps. Conversely, during the backward process, the trained diffusion model generates images by sequentially denoising the white noise.

Despite its success in generating high-quality images, diffusion models suffer from the drawbacks of prolonged inference time. Considerable interest has been expressed in minimizing the number of time steps during the sampling process to speed up generation, while preserving the quality of generated images. Such works include generalizing DDPM to non-Markovian processes (Song et al., 2021), deriving optimal variance during sampling (Bao et al., 2022b), thresholding the pixel values as additional regularization (Saharia et al., 2022a), or developing pseudo numerical methods for solving differential equations on manifolds (Liu et al., 2022a).

Though showing promising performance, few of them have theoretically and empirically examined the differences between the training and sampling process of DDPM. The training of DDPM involves maximizing the log-likelihood of the generated sample distribution to the ground truth sample distribution. This inherent requirement inevitably results in prediction errors during inference, attributable to the network's generalization capabilities. Moreover, a large number of diffusion

---

\*Equal Contribution

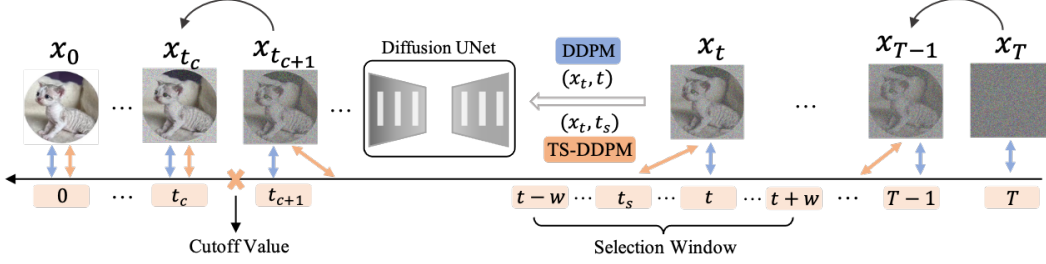


Figure 1: The comparison of TS-DDPM (ours) and DDPM. The orange and blue arrows denote the time-state coupling at each denoising step of TS-DDPM and DDPM, respectively. In TS-DDPM, we search for coupled time step within the selection window  $[t - w, t + w]$ , until the cutoff value  $t_c$ .

steps of DDPM ensures that small step sizes are taken, which guarantee the Gaussian assumption holds (Xiao et al., 2022). Consequently, a reduction in the number of time steps during the sampling phase can lead to larger prediction errors.

Moreover, if we take a closer look at the training of DDPM, at each time step  $t$ , ground truth samples  $x_0$  are given to produce corrupted samples  $x_t$  with noise  $\epsilon_t$ . The DDPM then takes both  $x_t$  and  $t$  as input to predict the noise  $\epsilon_t$ . In the context of sampling, one is required to synthesize data samples from white noise without the knowledge of the ground truth distributions. Coupled with the network prediction errors, this training-sampling discrepancy produces errors that progressively accumulate. This error accumulation phenomenon resembles the exposure bias (Ranzato et al., 2016; Schmidt, 2019) problem as identified in autoregressive generative models, given that the network is solely trained with the corrupted ground truth samples, rather than the network predicted samples.

The network prediction errors systematically exist in the current paradigm of DDPM training, which makes alternative sampling algorithms appealing. In this work, we focus on the exposure bias problem during sampling. Ning et al. (2023) propose to add perturbation to training samples to alleviate the exposure bias problem, which is sub-optimal since the retraining of DDPM that they required is computationally expensive, making it difficult to scale to high-resolution images. Since the time step is directly linked to the corruption level of the data samples, we theoretically and empirically show that by adjusting the next time step according to the variance of the current generated samples, one can effectively alleviate the exposure bias during sampling. We search for such a time step within a window  $t_w$  surrounding the current time step to restrict the denoising progress. Furthermore, based on the error patterns that the network makes on the training samples, we propose the use of a cutoff time step. For time steps larger than the cutoff time step, we search for the suitable time step within  $t_w$ . While for time steps smaller than the cutoff time step, we keep the original time step. Intuitively, it also suits the nature of DDPM, since the corruption level is smaller for small time steps. We refer to our sampling method as Time-Shift Sampler. Figure 1 presents a comparison of our method with the original DDPM.

In summary, our contributions are:

- We theoretically and empirically study the exposure bias problem of DDPM, which is often neglected by previous works.
- We propose a new sampling method called Time-Shift Sampler to alleviate the exposure bias problem, which avoids retraining the DDPM.
- Our Time-Shift Sampler shows significant improvements on commonly used image generation benchmarks, indicating the effectiveness of our framework.

## 2 Background: Denoising Diffusion Probabilistic Models

Denoising Diffusion probabilistic models (DDPMs) encompass a forward process which induces corruption in a data sample (e.g., an image) via Gaussian noise, and a corresponding inverse process aiming to revert this process in order to generate an image from standard Gaussian noise. Given a data distribution  $q(x_0)$  and a forward noise schedule  $\beta_t \in (0, 1)$ ,  $t = 1 \cdots T$ , the forward process is

structured as a Markov process, expressed as:

$$q(x_1 \dots T | x_0) = \prod_{t=1}^T q(x_t | x_{t-1}) \quad (1)$$

with the transition kernel  $q(x_t | x_{t-1}) = \mathcal{N}(x_t | \sqrt{\alpha_t} x_{t-1}, \beta_t \mathbf{I})$ , where  $\mathbf{I}$  denotes the identity matrix,  $\alpha_t$  and  $\beta_t$  are scalars and  $\alpha_t = 1 - \beta_t$ . The forward process, consequently, generates a sequence of noisy states, denoted as  $x_1, x_2, \dots, x_T$ . With a sufficiently large  $T$ , we achieve  $x_T \sim \mathcal{N}(\mathbf{0}, \mathbf{I})$ . Notably, the noisy intermediate state  $x_t$  only depends on  $x_0$  and parameter  $\bar{\alpha}_t$ , and  $x_t$  can be computed by marginalizing intermediate steps along the sequence:

$$q(x_t | x_0) = \mathcal{N}(x_t | \sqrt{\bar{\alpha}_t} x_0, (1 - \bar{\alpha}_t) \mathbf{I}) \quad (2)$$

where  $\bar{\alpha}_t = \prod_{i=1}^t \alpha_i$ . Moreover, the reparameterization trick allows us to sample  $x_t$  at any step  $t$  as:

$$x_t = \sqrt{\bar{\alpha}_t} x_0 + \sqrt{1 - \bar{\alpha}_t} \epsilon \quad (3)$$

where  $\epsilon \sim \mathcal{N}(\mathbf{0}, \mathbf{I})$ . Song et al. (2021) propose a more general non-Markov process bearing the same marginal distribution of  $x_t$  and index this process by  $\sigma_t$ :

$$\begin{aligned} q_\sigma(x_1 \dots T | x_0) &= q_\sigma(x_T | x_0) \prod_{t=2}^T q_\sigma(x_{t-1} | x_t, x_0) \\ q_\sigma(x_{t-1} | x_t, x_0) &= \mathcal{N}(x_{t-1} | \tilde{\mu}(x_t, x_0), \sigma_t^2) \\ \tilde{\mu}(x_t, x_0) &= \sqrt{\bar{\alpha}_{t-1}} x_0 + (\sqrt{1 - \bar{\alpha}_{t-1} - \sigma_t^2}) \frac{x_t - \sqrt{\bar{\alpha}_t} x_0}{\sqrt{1 - \bar{\alpha}_t}} \end{aligned} \quad (4)$$

The above equation encompasses two prevalent diffusion models, namely DDPM and DDIM when the  $\sigma_t^2$  is designated to  $\tilde{\beta}_t = \frac{\bar{\beta}_{t-1}}{\bar{\beta}_t} \beta_t$  and zero, respectively. The backward process can be regarded as a denoising process, which progressively eliminates noise from the current step  $x_t$  to obtain the previous state  $x_{t-1}$ , and finally reach  $x_0$ :

$$\begin{aligned} p(x_{0:T}) &= p(x_N) \prod_{t=1}^T p(x_{t-1} | x_t) \\ p(x_{t-1} | x_t) &= \mathcal{N}(x_{t-1} | \tilde{\mu}_t(x_t, \frac{1}{\sqrt{\bar{\alpha}_t}} (x_t + \sqrt{1 - \bar{\alpha}_t} \epsilon_t(x_t)))) \end{aligned} \quad (5)$$

During training phase, a time-dependent diffusion model is optimized by either learning the  $\tilde{\mu}_t$  or  $\epsilon_t$ . Empirically, it has been found (Ho et al., 2020) that the training works better by directly predicting  $\epsilon_t$ . The learning target is to optimize the variational lower bound of the negative log-likelihood, which could also be interpreted as minimizing the KL divergence between the forward and backward process. In practice, Ho et al. (2020) further simplified the loss function as:

$$\mathcal{L}_{simple} = \mathbb{E}_{t, x_0, \epsilon \sim \mathcal{N}(\mathbf{0}, \mathbf{I})} [\|\epsilon - \epsilon_\theta(\tilde{x}, t)\|_2^2] \quad (6)$$

where  $\tilde{x} = \sqrt{\bar{\alpha}_t} x_0 + \sqrt{1 - \bar{\alpha}_t} \epsilon$ . Upon the completion of the training of the diffusion model, we can sample a start state  $x_T \sim \mathcal{N}(\mathbf{0}, \mathbf{I})$  and adhere to the backward process to generate a data sample  $x_0$ . The training and inference processes are presented in algorithm 1 and 2, respectively.

---

**Algorithm 1** Training of DDPM

---

```

1: repeat
2:    $x_0 \sim q(x_0)$ 
3:    $t \sim \text{Uniform}(1, \dots, T)$ 
4:    $\epsilon \sim \mathcal{N}(\mathbf{0}, \mathbf{I})$  Compute  $x_t$  using Eq 3
5:   Take gradient descent step on
6:    $\nabla \|\epsilon - \epsilon_\theta(x_t)\|^2$ 
7: until converged

```

---



---

**Algorithm 2** Sampling of DDPM

---

```

1:  $x_T \sim \mathcal{N}(\mathbf{0}, \mathbf{I})$ 
2: for  $t = T, \dots, 1$  do
3:    $z \sim \mathcal{N}(\mathbf{0}, \mathbf{I})$  if  $t > 1$ , else  $z = 0$ 
4:    $x_{t-1} = \frac{1}{\sqrt{\bar{\alpha}_t}} (x_t - \frac{1 - \alpha_t}{\sqrt{1 - \bar{\alpha}_t}} \epsilon_\theta(x_t, t)) + \sigma_t z$ 
5: end for
6: return  $x_0$ 

```

---

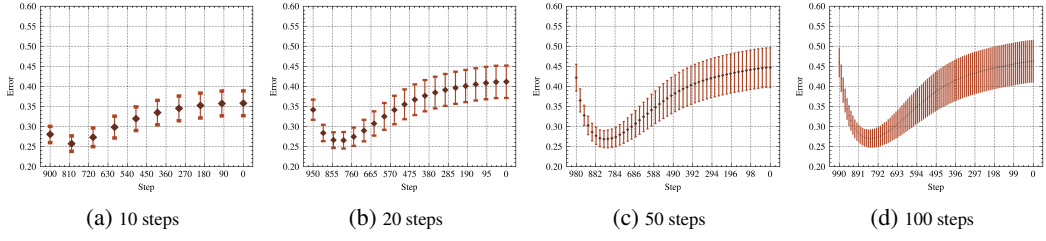


Figure 2: CIFAR-10 prediction errors of training samples for different number of sampling steps.

### 3 The Exposure Bias in Diffusion Models

In this section, we empirically demonstrate the exposure bias problem in Diffusion Models using CIFAR-10. We first study the evolution of prediction errors during sampling. Then we present the variance distribution of the corrupted samples by different time steps in the forward process.

Given a specific number of sampling steps, we compute the mean squared errors between the predicted samples and the ground truth samples at each step, as presented in Figure 2. It can be seen that the evolution of prediction errors adheres to a consistent pattern: initially decreasing before incrementally accumulating as the sampling process progresses. This phenomenon may be attributed to two possible factors: (1) The sampling process originates from white noise, which does not contain any information about the resultant sample distributions. Hence, in the initial stages, the errors are reduced as the white noise is rapidly shaped into a distribution that mirrors the ground truth sample distribution by Diffusion Models. (2) In the later stages, the exposure bias problem impacts the generated sample distributions. The network is still trying to predict distributions as authentic as possible; however, due to the training-sampling discrepancy, the network can only deduce such distributions from its own parameters and the generated sample distributions it obtained so far, without the guidance from the ground truth sample distributions, which leads to accumulated errors in Figure 2.

We also present the changes in variance of sample distributions for different time steps in Figure 3. At each step, we estimate the corrupted image samples with the network predicted noise using Equation 3. At time step 0, where no noise is added, ground truth images serve as the current samples. The distribution of the variance of the ground truth samples spans an approximate range of  $(0, 0.8)$ , showing the diversity of the sample distributions. As the noise is gradually added to the ground truth samples, the span of the variance becomes more and more narrow. Following 400 steps, the changes in the span range of the variance become stable, and gradually shift towards a narrow range surrounding the variance of white noise, which equals 1.0.

The evolution of the sample variance across different time steps indicates that the network exhibits a lower sensitivity to the early steps of the forward process of DDPM, as the variance of the samples can be distributed more sparsely within a broader range. Conversely, the network can be more sensitive to the later steps (e.g., after 400 steps), as we progressively approach white noise. The constricted variance range during the later stages implies that minor prediction errors during sampling can significantly impact overall performance.

### 4 Alleviating Exposure Bias via Time Step Shifting

In the backward process of DDPM, the transition kernel is assumed to adhere to a Gaussian distribution. To maintain this assumption, the difference between two successive steps must be sufficiently small, thereby necessitating the extensive training of DDPM with thousands of steps. The noise

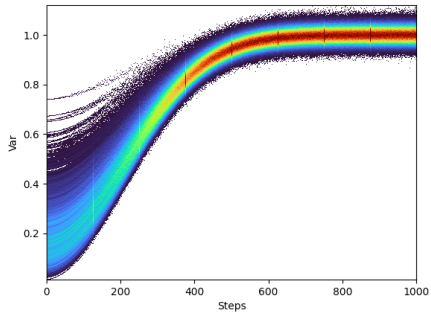


Figure 3: The density distribution of the variance of 5000 samples from CIFAR-10 by different time steps.

schedule defines the level of noise present at a specific time step within the diffusion process, as depicted in Equation 3. As previously discussed, the network prediction error coupled with discrepancy between training and inference phases inevitably results in the problem of exposure bias in DDPM. We introduce the  $\mathcal{C}(\tilde{x}_t, t)$ —referred to as the input couple for a trained diffusion model—to describe this discrepancy, which can be expressed as:

$$\mathcal{C}(\tilde{x}_t, t) = e^{-\text{dis}(\tilde{x}_t, x_t)} \quad (7)$$

where  $\tilde{x}_t$  and  $x_t$  represent the network input and ground truth states at time step  $t$  respectively, and  $\text{dis}(\cdot, \cdot)$  denotes the Euclidean distance. Consequently, during the training phase, the relationship  $\mathcal{C}(\tilde{x}_t, t) = 1$  holds true for all time steps, as the network always takes ground truth  $x_t$  as input. Moreover, a better couple  $\mathcal{C}(\tilde{x}_t, t)$  reduces the discrepancy between training and inference, thereby alleviating exposure bias. Previous works (Zhang et al., 2023a; Ning et al., 2023) have empirically and statistically affirmed that the network prediction error of DDPM follows a normal distribution. In conjunction with Equation 3, during the backward process at time step  $t$ , the predicted next state denoted as  $\hat{x}_{t-1}$  could be represented as:

$$\begin{aligned} \hat{x}_{t-1} &= x_{t-1} + \phi_{t-1} e_{t-1} \\ &= \sqrt{\alpha_{t-1}} x_0 + \sqrt{1 - \alpha_{t-1}} \epsilon_{t-1} + \phi_{t-1} e_{t-1} \\ &= \sqrt{\alpha_{t-1}} x_0 + \lambda_{t-1} \epsilon_{t-1} \end{aligned} \quad (8)$$

In this equation,  $\lambda_{t-1}^2 = \phi_{t-1}^2 + (1 - \alpha_{t-1})$ ,  $x_{t-1}$  denotes the ground truth at time step  $t-1$ ,  $\phi_{t-1} e_{t-1}$  represents the network prediction errors, and both  $e_{t-1}$  and  $\epsilon_{t-1}$  conform to a normal distribution. Upon observing that Equation 8 and Equation 3 share similar structure which is the ground truth  $x_0$  plus Gaussian noise with variable variance, we propose the subsequent assumption.

**Assumption 4.1** *During the inference phase at time step  $t$ , the next state predicted by the network  $\hat{x}_{t-1}$ , may not optimally align with time step  $t-1$  within the context of the pretrained diffusion model. In other words, there might be an alternate time step  $t_s$ , that potentially couples better with  $\hat{x}_{t-1}$ :*

$$\exists s \in \{1 \cdots T\}, \quad \text{s.t.} \quad \mathcal{C}(\hat{x}_{t-1}, t_s) \geq \mathcal{C}(\hat{x}_{t-1}, t-1) \quad (9)$$

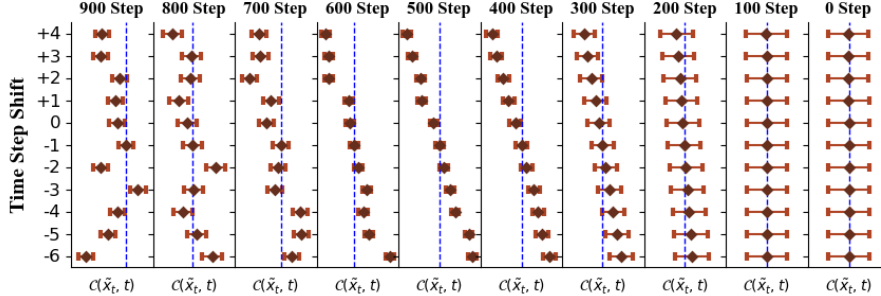


Figure 4: The training and inference discrepancy of DDIM with 10 sampling steps on CIFAR-10. The dashed line in each column denotes the couple of predicted  $\hat{x}_t$  and  $t$ . Points on the right side of the dashed line means that the corresponding time steps couple better with  $\hat{x}_t$  than time step  $t$ .

To verify our assumption, we initially conduct a statistical examination of the discrepancy between training and inference in a pretrained diffusion model. A sample size of 5000 instances was randomly selected from the CIFAR-10 training set and Equation 3 was utilized to generate ground truth states  $x_t$  for a sequence of time steps. Subsequently, we compare the  $\mathcal{C}(\hat{x}_{t-1}, t-1)$  with  $\mathcal{C}(x_s, t-1)$ . Here we show the results of 10 inference steps in the backward process and only consider time step  $t_s$  within the range of  $t-6$  to  $t+4$ . As depicted in Figure 4, for certain backward steps, there are alternate time steps  $t_s$  that display a stronger correlation with the predicted next state  $\hat{x}_{t-1}$  compared to time step  $t-1$ . We also observe that when approaching the zero time step, all nearby time steps converge to the same distribution. Similar findings were observed for other pretrained diffusion models on different datasets including Celeba-A and ImageNet-64x64 with varying settings, such as different numbers of inference steps and ranges of  $t_s$ . These results are further elaborated in Appendix C.

Our empirical findings lend substantial support to Assumption 4.1. This naturally prompts the question: How can we identify the time step that best couples with the predicted  $\hat{x}_{t-1}$ ? By optimizing the KL divergence between the predicted  $\hat{x}_{t-1}$  and  $x_s$  at time step  $t_s$ , we arrive at the following Theorem 4.1, with the complete derivation provided in Appendix F.

**Theorem 4.1** *Given state  $\hat{x}_t$  and assuming the predicted next state is  $\hat{x}_{t-1}$ , the optimal time step  $t_s$  among those closely surrounding  $t-1$ , which best couples with  $\hat{x}_{t-1}$ , is determined to have the following variance:*

$$\sigma_s \approx \text{Tr}(\hat{\Sigma}_{t-1}) + \frac{1}{d} \|e\|^2 \approx \sigma_{t-1} - \frac{\|e\|^2}{d(d-1)} \quad (10)$$

where  $d$  is the dimension of the input,  $e$  represents the network prediction error,  $\hat{\Sigma}_{t-1}$  is the per-dimension covariance matrix of the predicted  $\hat{x}_{t-1}$ , and  $\sigma_t$  is the variance of predicted  $\hat{x}_{t-1}$ .

The derivation of Theorem 4.1 mainly follows two steps: Firstly, we optimize the KL divergence between  $x_s$  and  $\hat{x}_{t-1}$  to obtain the variance of  $x_s$ ; Secondly, we establish the relationship between the covariance matrix of the  $\hat{x}_{t-1}$  distribution and the variance of the predicted  $\hat{x}_{t-1}$ . The results articulated in Theorem 4.1 could be further simplified to  $\sigma_s \approx \sigma_{t-1}$ , given the assumption that the network prediction error at the current time step is minimal. This assumption has been found to hold well in practice. Based on findings of Theorem 4.1, we propose the Time-Shift Sampler, a methodology that can be seamlessly incorporated into existing sampling algorithms, such as Denoising Diffusion Implicit Models (DDIM) and Denoising Diffusion Probabilistic Models (DDPM). We name our algorithm as Time-Shift DDIM (TS-DDIM) and Time-Shift DDPM (TS-DDPM). And in light of the earlier discussion that the model’s prediction of nearby time steps tends to converge to the same distribution during the later stage of the inference process, we further augment our algorithm with a cutoff mechanism, in which we remove the time-shift operation when the time step is smaller than a predefined cutoff time step. Our algorithm is detailed in Algorithm 3

## 5 Experiments

We compare our TS-DDIM/DDPM to the original DDIM (Song et al., 2021) and DDPM (Ho et al., 2020), with  $\sigma^2 = \tilde{\beta}_n$  and  $\sigma^2 = 0$  respectively. Following DDIM, we consider two types of time step selection procedures during sampling, namely *uniform* and *quadratic*. We conduct experiments using pre-trained models on CIFAR-10 (Krizhevsky, 2009), CelebA 64×64 (Liu et al., 2015) and ImageNet 64×64 (Deng et al., 2009). We adopt the pre-trained models trained with linear schedule (LS) (Ho et al., 2020). We conduct experiments for varying sampling time steps, namely 5, 10, 20, 50, and 100. We use the Frechet Inception Distance (FID (Heusel et al., 2017)) for evaluating the quality of the generated images. The detailed experimental setups are provided in Appendix A.

The window size is selected according to the step sizes given a number of sampling time steps. For fewer sampling steps, a larger window size is preferred. An ablation study on window size selection is presented in Sec.6.2. The cutoff value is selected according to the variance distribution of training samples as depicted in Figure 3. Specifically, we select the cutoff value within the range of [200, 400] for the model is more sensitive to larger time steps, and more tolerant to noise for smaller time steps. The selection of cutoff value is also dependent to the number of sampling steps we take, as some cutoff values are equivalent to specific time steps (e.g. 200 and 250 are equivalent to models sampling with 10 steps using *uniform* time step selection). We further discuss it in Sec. 6.3.

---

### Algorithm 3 TS-DDIM/DDPM

---

```

1: Input : Trained diffusion model  $\epsilon_\theta$ ; Window size  $w$ ; Reverse Time series  $\{T, T - \tau_i, \dots, 0\}$ ; Cutoff threshold  $c$ 
2: Initialize:  $x_T \sim \mathcal{N}(\mathbf{0}, \mathbf{I})$ ;  $t_s = -1$ 
3: for  $t = T, T - \tau_i, \dots, 0$  do
4:    $t_{next} = t$ , If  $t_s \neq -1$  else  $t_{next} = t_s$ 
5:    $z \sim \mathcal{N}(\mathbf{0}, \mathbf{I})$ , if  $t > 1$  else  $z = \mathbf{0}$ 
6:    $\epsilon_t = \epsilon_\theta(x_t, t_{next})$ 
7:   take a DDIM/DDPM step to get  $x_{t-1}$ 
8:   if  $t > c$  then
9:     Get variance of window steps:  $\Sigma = \{1 - \bar{\alpha}_{t-w}, 1 - \bar{\alpha}_{t-w+1}, \dots, 1 - \bar{\alpha}_{t+w}\}$ 
10:     $t_s = \arg \min_t \|var(x_{t-1})\mathbf{I} - \Sigma\|$ 
11:    else
12:       $t_s = -1$ 
13:    end if
14:  end for
15: return  $x_0$ 

```

---

## 6 Results

### 6.1 Main Results

Dataset	Sampling Method	5 steps	10 steps	20 steps	50 steps	100 steps
CIFAR-10	DDIM ( <i>quadratic</i> )	41.57	13.70	6.91	4.71	4.23
	TS-DDIM( <i>quadratic</i> )	<b>38.09</b>	<b>11.93</b>	<b>6.12</b>	<b>4.16</b>	<b>3.81</b>
	DDIM( <i>uniform</i> )	44.60	18.71	11.05	7.09	5.66
	TS-DDIM( <i>uniform</i> )	<b>35.13</b>	<b>12.21</b>	<b>8.03</b>	<b>5.56</b>	<b>4.56</b>
CelebA	DDPM ( <i>uniform</i> )	83.90	42.04	24.60	14.76	10.66
	TS-DDPM ( <i>uniform</i> )	<b>67.06</b>	<b>33.36</b>	<b>22.21</b>	<b>13.64</b>	<b>9.69</b>
	DDIM ( <i>quadratic</i> )	27.28	10.93	6.54	5.20	4.96
	TS-DDIM ( <i>quadratic</i> )	<b>24.24</b>	<b>9.36</b>	<b>5.08</b>	<b>4.20</b>	<b>4.18</b>
ImageNet	DDIM ( <i>uniform</i> )	24.69	17.18	13.56	9.12	6.60
	TS-DDIM ( <i>uniform</i> )	<b>21.32</b>	<b>10.61</b>	<b>7.01</b>	<b>5.29</b>	<b>6.50</b>
	DDPM ( <i>uniform</i> )	42.83	34.12	26.02	18.49	13.90
	TS-DDPM ( <i>uniform</i> )	<b>33.87</b>	<b>27.17</b>	<b>20.42</b>	<b>13.54</b>	<b>12.83</b>
ImageNet	DDIM ( <i>uniform</i> )	146.19	42.51	25.60	<b>20.17</b>	18.76
	TS-DDIM ( <i>uniform</i> )	<b>140.89</b>	<b>41.68</b>	<b>25.32</b>	20.26	<b>17.20</b>
	DDPM ( <i>uniform</i> )	96.99	62.90	35.72	21.47	18.27
	TS-DDPM ( <i>uniform</i> )	<b>95.76</b>	<b>61.78</b>	<b>34.83</b>	<b>20.35</b>	<b>17.70</b>

Table 1: Quality of the image generation measured with FID  $\downarrow$  on CIFAR-10 ( $32 \times 32$ ), CelebA ( $64 \times 64$ ) and ImageNet ( $64 \times 64$ ) with varying time steps for different sampling algorithms.

In Table 1, we report the results of our TS-DDIM/DDPM sampling method compared with those obtained with DDIM and DDPM, where we vary the time steps and the time step selection procedures. We take larger window sizes for fewer sampling steps. The cutoff value is within the range of [200, 400], and is dependent to the number of time steps we take. As expected, our TS-DDIM/DDPM nearly consistently improves the quality of the generated images with respect to that of the original DDIM and DDPM. We observe that for time steps less than 20 with *uniform* time step selection, the performance improvements are extremely significant as compared to the original DDIM/DDPM. We implement time shifts only for time steps exceeding the cutoff value. The *uniform* selection includes more large time steps than the *quadratic* selection, providing the model with more opportunities for correction and thus resulting in greater improvement. However, our algorithm shows less enhancement on the ImageNet dataset compared to others. This could potentially be attributed to the unique training setting of the DDPM model on ImageNet, which uses 4000 time steps instead of 1000 used for the other datasets. Models trained with larger time steps experience a more extensive range of noisy inputs. Consequently, this could result in a model that is more robust to noisy inputs during inference.

### 6.2 Influence of Window Size

We conduct a study on the effect of window sizes. The results are presented in Figure 5, where we fix the cutoff value=300, and vary the window sizes for different numbers of sampling steps. In the assessment of 10 and 20 sampling steps, larger window sizes (up to 60 for sampling with 10 steps) are evaluated to ensure an adequate search space for a suitable time step. Contrastingly, in the context of 50 and 100 sampling steps, a comparative analysis is undertaken involving smaller window sizes, given the limitation of step size to under 20 and 10 respectively. We observe that with a lack of overlapping time steps (i.e., when window size is smaller than step size), the maximum window size does not consistently yield optimal results. To illustrate, when considering 20 sampling steps, a window size of 50 underperforms in comparison to a model employing a window size of 40. Such observation might be attributed to the less accurate estimations of time shifts, precipitated by the network’s

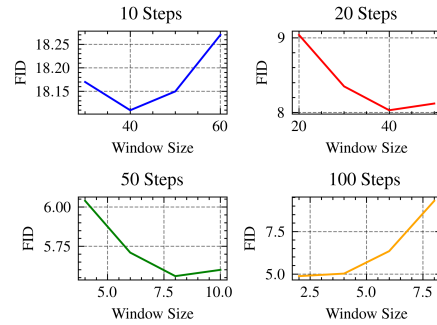


Figure 5: The impact of different window sizes on the quality of generated CIFAR-10 images with *uniform* time step selection with cutoff value=300.

inaccurate predictions in scenarios involving fewer sampling steps. However, when the number of sampling steps is increased, such as in a configuration of 100 steps, it is recommended to opt for a smaller window size, due to the enhanced accuracy of per-step predictions achievable with smaller step sizes. In summary, it can be deduced that larger window sizes are more effective for fewer sampling steps, whereas smaller window sizes tend to perform better when the number of sampling steps is increased.

### 6.3 Influence of the Cutoff Value

The results on the impact of different cutoff values on the image generation performance on CIFAR-10 are presented in Figure 6 (a similar study on other datasets can be found in Appendix D). From the density distribution plot of the sample variance, we can have a good estimation of the range of the cutoff values to be within [200, 400]. As shown in Figure 6, the best FID is reached with cutoff value=200 for 10 sampling steps, while for the other sampling steps the best FID is reached with cutoff value=300. One possible reason for the different pattern with 10 sampling step is that the step size is much larger (100 vs.  $< 50$ ), which makes additional time-shift operations beneficial. For 20, 50 and 100 sampling steps, though we observe a similar pattern in changes of FID, the effect of the cutoff value is more drastic for fewer sampling steps. For 100 sampling steps, the effect of changing cutoff value from 200 to 300 is minimal (FID: 4.91  $\rightarrow$  4.88). Based on the observations, we can conclude that cutoff values are more effective when dealing with fewer sampling steps where the model takes larger step sizes to make predictions. And generally cutoff value=300 works best for sufficiently enough (e.g.  $> 10$ ) time steps.

### 6.4 Discussion

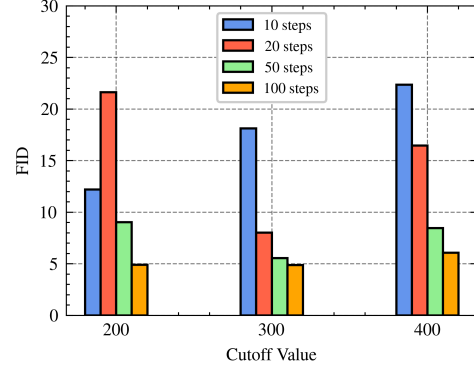


Figure 6: The impact of different cutoff values on the quality of generated CIFAR-10 images with *uniform* time step selection. We adopt window size= {40;30;8;2} for {10;20;50;100} steps

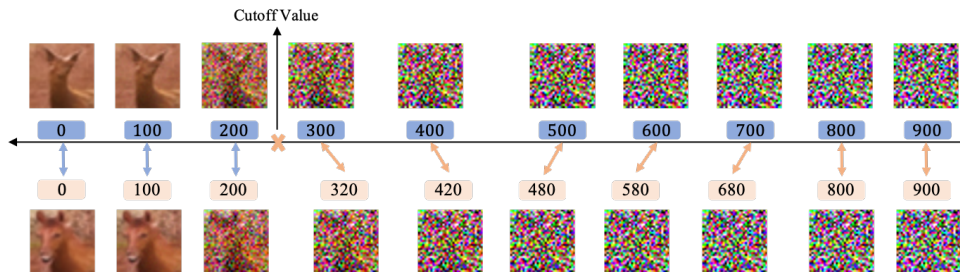


Figure 7: Example of generation process of TS-DDIM and DDIM on CIFAR-10. We use the horizontal black arrow to represent the time line, with the DDIM generation chain above it, TS-DDIM generation chain underneath it. We sample 10 steps with window  $[t - 20, t + 20]$  and cutoff value=200.

The proposed novel sampling method is motivated by the theoretical and empirical analysis of the exposure bias problem in DDPM. Experimental results show that our sampling method can effectively improve the quality of the generated images compared to images generated with the original DDIM/DDPM models quantitatively measured with the FID score. We present the comparison of the generation chain of TS-DDIM (our model) and DDIM in Figure 7. It can be seen that TS-DDIM shifted most of the time steps before reaching the cutoff value, which yields much better generation quality of the image of a horse. Additional qualitative examples will be presented in the Appendix E. Moreover, Ning et al. (2023) tackle the exposure bias problem in DDPM by adding input perturbation during training, which makes it computationally expensive for high-resolution images. In Appendix E, we present results of our method on LSUN-bedroom (256  $\times$  256) (Yu et al., 2016), which ADM-IP (Ning et al., 2023) does not explore due to limited resources.

## 7 Related Work

**Denoising Diffusion Probabilistic Model.** The denoising diffusion probabilistic model (DDPM) was first introduced by Sohl-Dickstein et al. (2015) and further advanced by Nichol and Dhariwal (2021), where they include variance learning in the model and optimize it with a new weighted variational bound. Song et al. (2020) further connect DDPMs with stochastic differential equations by considering DDPMs with infinitesimal timesteps. They also find that both score-based generative models (Song and Ermon, 2019) and DDPMs can be formulated by stochastic differential equations with different discretization. Some variants of DDPMs are introduced recently, including the variational diffusion model (VDM) Kingma et al. (2021) that also learns the forward process, and consistency model (Song et al., 2023) and rectified flow model (Liu et al., 2022b), both of which aim to learn to generate natural images in one inference step.

DDPMs are initially applied in the pixel space achieving impressive success in generating images of high quality, however, they suffer from the significant drawbacks such as prolonged inference time and substantial training cost. Rombach et al. (2022b) propose to use a diffusion model in the latent image space, which drastically reduces the computational time and training cost. DDPMs have been widely used in different fields, for example controllable image generation (Rombach et al., 2022b; Choi et al., 2021; Zhang and Agrawala, 2023; Mou et al., 2023), language generation (Zhang et al., 2023b; Ye et al., 2023; Lin et al., 2022), image super-resolution (Saharia et al., 2022b) and video generation (Hu et al., 2023; Karras et al., 2023; He et al., 2022).

**DDPM Accelerator.** Though diffusion models have shown powerful generation performance, it normally takes hundreds of steps to generate high-quality images (Ho et al., 2020). To accelerate the generation speed, Song et al. (2021) propose the denoising diffusion implicit model (DDIM) which derives ordinary differential equations for the diffusion model showing that it is possible to generate high-quality images in much less steps. Liu et al. (2022a) introduce different numerical solvers to further reduce the number of generation steps. Bao et al. (2022b) surprisingly find that the variance in the backward process can be analytically computed and improve the generation speed and quality of the generated images. Bao et al. (2022a) also attempt to further remove the diagonal variance matrix assumption and boost the image generation performance. Lu et al. (2022) leverage a high-order ordinary differential equations solver to reduce the generation steps of a diffusion model to 10, while maintaining the image quality. We follow this line of research that reduces the generation steps but propose a method to better select them.

## 8 Limitation and Conclusion

### 8.1 Limitation and Future Work.

In this work, we introduce the Time-Shift Sampler, a training-free mechanism devised to mitigate the exposure bias problem inherent to the diffusion model, thereby enhancing the quality of generated images. Despite its efficacy, our sampler suffers from the limitation that it introduces two parameters, i.e., window size and cutoff value. We estimated their values based on the statistical analysis of training data. However, more advanced methods to analytically derive the optimal value of these two parameters might be possible since both the cutoff value and the window size are related to the noise level of each step. We leave this further exploration to future work. We also foresee possibilities to use the concept of the Time-Shift Sampler in other Markovian processes where a reduction in processing steps is desired.

### 8.2 Conclusion

In this paper, we undertake a statistical and theoretical examination of the issue of error accumulation, also known as exposure bias, within the probabilistic diffusion models. Different from previous work, which tries to reduce exposure bias by retraining diffusion model with extra noisy inputs, we demonstrate that this bias can be mitigated by identifying the timestep that most aligns with the subsequent predicted step. Furthermore, we theoretically derive the variance of this optimal next timestep. Leveraging these insights, we introduce a novel and training-free inference algorithm, the Time-Shifted Sampler, to alleviate exposure bias in diffusion models. Our algorithm can be seamlessly incorporated into existing sampling algorithms for diffusion models including DDPM and DDIM. Extensive experimental results prove the effectiveness of our method.

## References

Bao, F., Li, C., Sun, J., Zhu, J., and Zhang, B. (2022a). Estimating the optimal covariance with imperfect mean in diffusion probabilistic models. *arXiv preprint arXiv:2206.07309*.

Bao, F., Li, C., Zhu, J., and Zhang, B. (2022b). Analytic-DPM: an analytic estimate of the optimal reverse variance in diffusion probabilistic models. In *International Conference on Learning Representations*.

Choi, J., Kim, S., Jeong, Y., Gwon, Y., and Yoon, S. (2021). Ilvr: Conditioning method for denoising diffusion probabilistic models. *arXiv preprint arXiv:2108.02938*.

Deng, J., Dong, W., Socher, R., Li, L.-J., Li, K., and Fei-Fei, L. (2009). Imagenet: A large-scale hierarchical image database. In *2009 IEEE Conference on Computer Vision and Pattern Recognition*, pages 248–255. Curran Associates, Inc.

Dhariwal, P. and Nichol, A. (2021). Diffusion models beat gans on image synthesis. In Ranzato, M., Beygelzimer, A., Dauphin, Y., Liang, P., and Vaughan, J. W., editors, *Advances in Neural Information Processing Systems*, volume 34, pages 8780–8794. Curran Associates, Inc.

He, Y., Yang, T., Zhang, Y., Shan, Y., and Chen, Q. (2022). Latent video diffusion models for high-fidelity video generation with arbitrary lengths. *arXiv preprint arXiv:2211.13221*.

Heusel, M., Ramsauer, H., Unterthiner, T., Nessler, B., and Hochreiter, S. (2017). Gans trained by a two time-scale update rule converge to a local nash equilibrium. In Guyon, I., Luxburg, U. V., Bengio, S., Wallach, H., Fergus, R., Vishwanathan, S., and Garnett, R., editors, *Advances in Neural Information Processing Systems*, volume 30. Curran Associates, Inc.

Ho, J., Jain, A., and Abbeel, P. (2020). Denoising diffusion probabilistic models. *Advances in Neural Information Processing Systems*, 33:6840–6851.

Hu, Y., Chen, Z., and Luo, C. (2023). Lamd: Latent motion diffusion for video generation. *arXiv preprint arXiv:2304.11603*.

Karras, J., Holynski, A., Wang, T.-C., and Kemelmacher-Shlizerman, I. (2023). Dreampose: Fashion image-to-video synthesis via stable diffusion. *arXiv preprint arXiv:2304.06025*.

Kingma, D., Salimans, T., Poole, B., and Ho, J. (2021). Variational diffusion models. *Advances in neural information processing systems*, 34:21696–21707.

Krizhevsky, A. (2009). Learning multiple layers of features from tiny images. Technical report, University of Toronto.

Lin, Z., Gong, Y., Shen, Y., Wu, T., Fan, Z., Lin, C., Chen, W., and Duan, N. (2022). Genie: Large scale pre-training for text generation with diffusion model. *arXiv preprint arXiv:2212.11685*.

Liu, L., Ren, Y., Lin, Z., and Zhao, Z. (2022a). Pseudo numerical methods for diffusion models on manifolds. In *International Conference on Learning Representations*.

Liu, X., Gong, C., and Liu, Q. (2022b). Flow straight and fast: Learning to generate and transfer data with rectified flow. *arXiv preprint arXiv:2209.03003*.

Liu, Z., Luo, P., Wang, X., and Tang, X. (2015). Deep learning face attributes in the wild. In *Proceedings of the IEEE International Conference on Computer Vision (ICCV)*.

Lu, C., Zhou, Y., Bao, F., Chen, J., Li, C., and Zhu, J. (2022). Dpm-solver: A fast ode solver for diffusion probabilistic model sampling in around 10 steps. *arXiv preprint arXiv:2206.00927*.

Mou, C., Wang, X., Xie, L., Zhang, J., Qi, Z., Shan, Y., and Qie, X. (2023). T2i-adapter: Learning adapters to dig out more controllable ability for text-to-image diffusion models. *arXiv preprint arXiv:2302.08453*.

Nichol, A. Q. and Dhariwal, P. (2021). Improved denoising diffusion probabilistic models. In *International Conference on Machine Learning*, pages 8162–8171. PMLR.

Nichol, A. Q., Dhariwal, P., Ramesh, A., Shyam, P., Mishkin, P., McGrew, B., Sutskever, I., and Chen, M. (2022). GLIDE: Towards photorealistic image generation and editing with text-guided diffusion models. In Chaudhuri, K., Jegelka, S., Song, L., Szepesvari, C., Niu, G., and Sabato, S., editors, *Proceedings of the 39th International Conference on Machine Learning*, volume 162 of *Proceedings of Machine Learning Research*, pages 16784–16804. PMLR.

Ning, M., Sangineto, E., Porrello, A., Calderara, S., and Cucchiara, R. (2023). Input perturbation reduces exposure bias in diffusion models. *arXiv preprint arXiv:2301.11706*.

Ramesh, A., Dhariwal, P., Nichol, A., Chu, C., and Chen, M. (2022). Hierarchical text-conditional image generation with clip latents.

Ranzato, M., Chopra, S., Auli, M., and Zaremba, W. (2016). Sequence level training with recurrent neural networks. In Bengio, Y. and LeCun, Y., editors, *4th International Conference on Learning Representations, ICLR 2016, San Juan, Puerto Rico, May 2-4, 2016, Conference Track Proceedings*.

Rombach, R., Blattmann, A., Lorenz, D., Esser, P., and Ommer, B. (2022a). High-resolution image synthesis with latent diffusion models. In *Proceedings of the IEEE/CVF Conference on Computer Vision and Pattern Recognition (CVPR)*, pages 10684–10695.

Rombach, R., Blattmann, A., Lorenz, D., Esser, P., and Ommer, B. (2022b). High-resolution image synthesis with latent diffusion models. In *Proceedings of the IEEE/CVF Conference on Computer Vision and Pattern Recognition*, pages 10684–10695.

Saharia, C., Chan, W., Saxena, S., Li, L., Whang, J., Denton, E., Ghasemipour, S. K. S., Gontijo-Lopes, R., Ayan, B. K., Salimans, T., Ho, J., Fleet, D. J., and Norouzi, M. (2022a). Photorealistic text-to-image diffusion models with deep language understanding. In Oh, A. H., Agarwal, A., Belgrave, D., and Cho, K., editors, *Advances in Neural Information Processing Systems*.

Saharia, C., Ho, J., Chan, W., Salimans, T., Fleet, D. J., and Norouzi, M. (2022b). Image super-resolution via iterative refinement. *IEEE Transactions on Pattern Analysis and Machine Intelligence*.

Schmidt, F. (2019). Generalization in generation: A closer look at exposure bias. In *Proceedings of the 3rd Workshop on Neural Generation and Translation*, pages 157–167, Hong Kong. Association for Computational Linguistics.

Sohl-Dickstein, J., Weiss, E., Maheswaranathan, N., and Ganguli, S. (2015). Deep unsupervised learning using nonequilibrium thermodynamics. In *International Conference on Machine Learning*, pages 2256–2265. PMLR.

Song, J., Meng, C., and Ermon, S. (2021). Denoising diffusion implicit models. In *International Conference on Learning Representations*.

Song, Y., Dhariwal, P., Chen, M., and Sutskever, I. (2023). Consistency models. *arXiv preprint arXiv:2303.01469*.

Song, Y. and Ermon, S. (2019). Generative modeling by estimating gradients of the data distribution. *Advances in neural information processing systems*, 32.

Song, Y., Sohl-Dickstein, J., Kingma, D. P., Kumar, A., Ermon, S., and Poole, B. (2020). Score-based generative modeling through stochastic differential equations. *arXiv preprint arXiv:2011.13456*.

Xiao, Z., Kreis, K., and Vahdat, A. (2022). Tackling the generative learning trilemma with denoising diffusion GANs. In *International Conference on Learning Representations*.

Ye, J., Zheng, Z., Bao, Y., Qian, L., and Wang, M. (2023). Dinoiser: Diffused conditional sequence learning by manipulating noises.

Yu, F., Seff, A., Zhang, Y., Song, S., Funkhouser, T., and Xiao, J. (2016). Lsun: Construction of a large-scale image dataset using deep learning with humans in the loop.

Zhang, G., Kenta, N., and Kleijn, W. B. (2023a). Lookahead diffusion probabilistic models for refining mean estimation. *arXiv preprint arXiv:2304.11312*.

Zhang, H., Liu, X., and Zhang, J. (2023b). Diffusum: Generation enhanced extractive summarization with diffusion. *arXiv preprint arXiv:2305.01735*.

Zhang, L. and Agrawala, M. (2023). Adding conditional control to text-to-image diffusion models. *arXiv preprint arXiv:2302.05543*.

## 9 Appendix

### A Additional Experimental Setup

Following DDIM (Song et al., 2021), we use two types of time step selection procedures, namely *uniform* and *quadratic*. For  $t_i < T$ :

- *uniform*: we select time steps such that  $t_i = \lfloor ci \rfloor$ , for a constant value  $c$
- *quadratic*: we select time steps such that  $t_i = \lfloor ci^2 \rfloor$ , for a constant value  $c$

The architecture of our models follows the one of DDPM (Ho et al., 2020). For all datasets, we use the same pretrained models for evaluating the sampling methods. For CIFAR-10 and LSUN-bedroom, we obtain the checkpoints from the original DDPM implementation; for CelebA, we adopt the DDIM checkpoints; for ImageNet, we use the guided diffusion (Dhariwal and Nichol, 2021) checkpoints.

### B Error Analysis

We provide here more examples of prediction errors on training samples for different sampling steps for the different datasets. Figure 8 presents the prediction errors obtained in the CelebA dataset, which show similar pattern as those of the CIFAR-10 dataset as depicted in Figure 2.

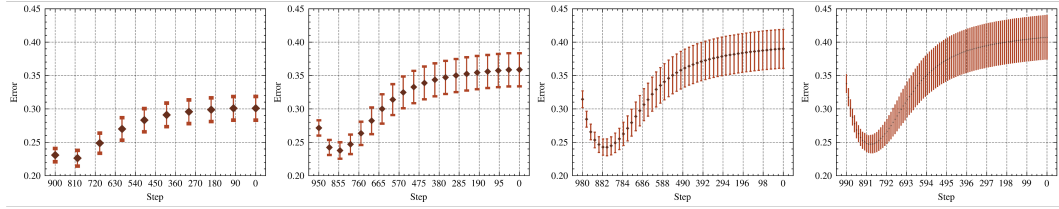


Figure 8: CelebA prediction errors of training samples for different number of sampling steps.

### C Training-Inference Discrepancy

We provide more examples on the training-inference discrepancy for the different datasets in Figure 9a, 9b, 16 and 17. For varying numbers of time steps, the same training-inference discrepancy pattern can be observed as in Figure 4. Specifically, for a certain backward step  $t$ , given a time step window  $[t - w, t + w]$  surrounding  $t$ , there exists a time step  $t_s$  that might couple better with the predicted next state  $\hat{x}_{t-1}$ . And as sampling progresses, the coupling effects for  $\hat{x}_{t-1}$  become identical for surrounding time steps.

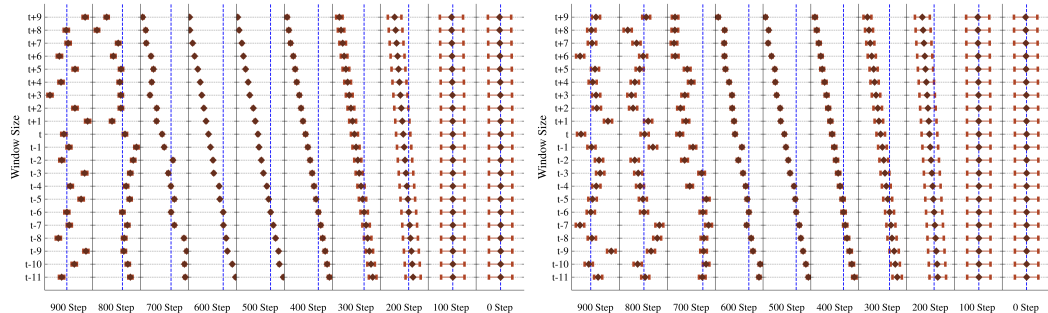


Figure 9: The training and inference discrepancy of DDIM with 10 sampling steps for window size=20: Left: CelebA dataset; Right: CIFAR-10 dataset.

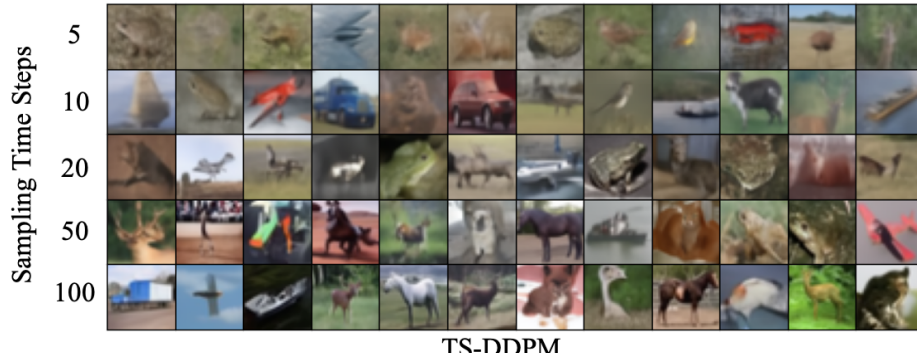


Figure 10: CIFAR-10 samples for varying time steps using TS-DDPM.

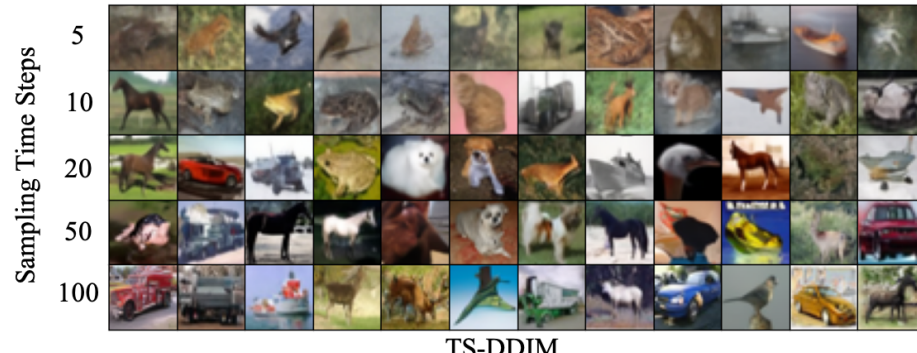


Figure 11: CIFAR-10 samples for varying time steps using TS-DDIM.

## D Qualitative Examples

In this section we present the example images generated using different sampling method with *uniform* time selection procedure for varying sampling time steps. Generated examples can be found in Figure 10, 11, 12, 13, 14 and 15. It can be seen that we can generate images with good quality for less than 10 sampling steps.

## E Additional Results

We present more results on LSUN-bedroom (Yu et al., 2016) in Table 2. Limited by computational resources, we do not properly tune the parameters, i.e., window size and cutoff values, for the LSUN-bedroom. We leave the exploration of a more efficient tuning strategy on high-resolution images for future work.

Dataset	Sampling Method	5 steps	10 steps	20 steps	50 steps
LSUN-bedroom	DDIM( <i>uniform</i> )	52.29	16.90	8.78	<b>6.74</b>
	TS-DDIM( <i>uniform</i> )	<b>51.57</b>	<b>16.66</b>	<b>8.29</b>	6.90
	DDPM ( <i>uniform</i> )	85.60	42.82	22.66	10.79
	TS-DDPM ( <i>uniform</i> )	<b>79.05</b>	<b>32.47</b>	<b>15.40</b>	<b>10.20</b>

Table 2: Quality of the image generation measured with  $\text{FID} \downarrow$  on LSUN-bedroom ( $256 \times 256$ ) with varying time steps for different sampling algorithms.

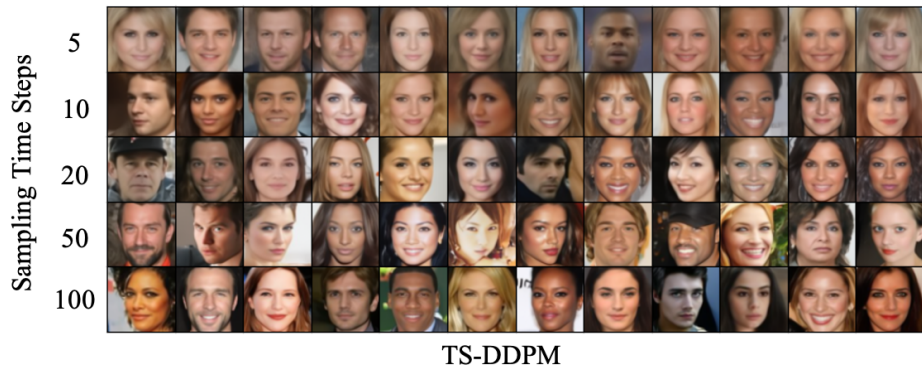


Figure 12: CelebA samples for varying time steps using TS-DDPM.

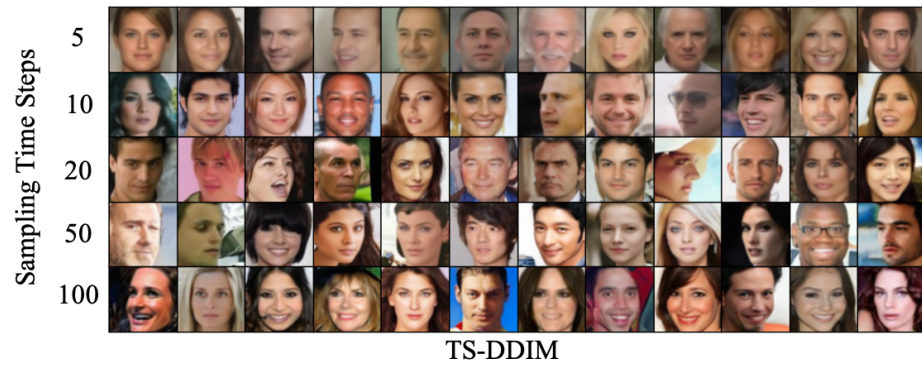


Figure 13: CelebA samples for varying time steps using TS-DDIM.



Figure 14: LSUN-bedroom samples for varying time steps using TS-DDPM.

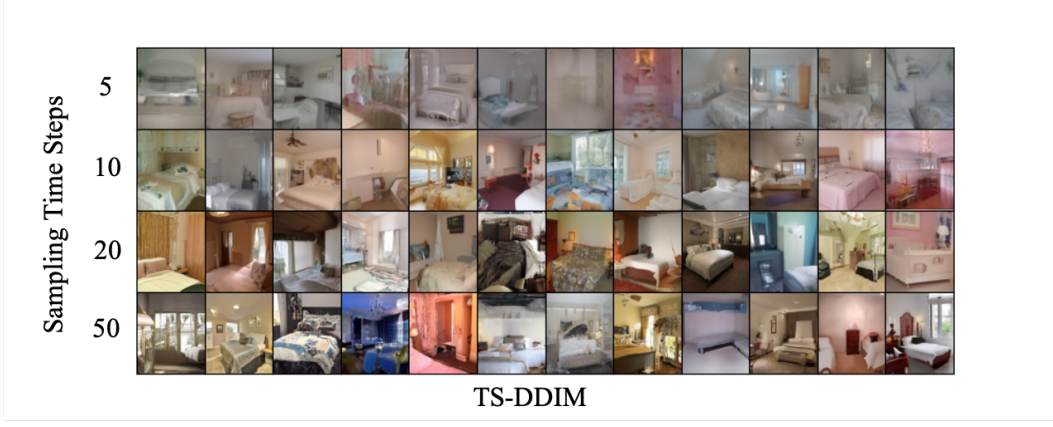


Figure 15: LSUN-bedroom samples for varying time steps using TS-DDIM.

## F Derivation

In this section, we prove the Theorem 4.1.

*proof.* We first find the optimal time step  $t_s$  by minimizing the KL divergence between  $\hat{x}_{t-1}$  and  $x_s$ . As  $q(x_s|x_0) = \mathcal{N}(x_s|\sqrt{\bar{\alpha}_t}x_0, (1-\bar{\alpha}_t)\mathbf{I})$  and assume  $p(\hat{x}_{t-1}|\hat{x}_t)$  is a probability density function of the distribution for  $\hat{x}$  with mean  $\hat{u}_{t-1}$  and covariance matrix  $\hat{\Sigma}_{t-1}$ , then according to Lemma 2. of Bao et al. (2022b), we have:

$$\begin{aligned}
& \mathcal{D}_{KL}(p(\hat{x}_{t-1}|\hat{x}_t)||q(x_s|x_0)) \\
&= \mathcal{D}_{KL}(\mathcal{N}(x|\hat{u}_{t-1}, \hat{\Sigma}_{t-1})||\mathcal{N}(\mu_s, \Sigma_s)) + \mathcal{H}(\mathcal{N}(x|\hat{u}_{t-1}, \hat{\Sigma}_{t-1})) - \mathcal{H}(p(\hat{x}_{t-1}|\hat{x}_t)) \\
&= \frac{1}{2}(\log(|\Sigma_s|) + \text{Tr}(\Sigma_s^{-1}\hat{\Sigma}_{t-1}) + (\hat{u}_{t-1} - \mu_s)\Sigma_s^{-1}(\hat{u}_{t-1} - \mu_s)^T) + C \\
&= \frac{1}{2}(d\log(1-\bar{\alpha}_s) + \frac{d}{1-\bar{\alpha}_s}\text{Tr}(\hat{\Sigma}_{t-1}) + \frac{1}{1-\bar{\alpha}_s}\|\hat{u}_{t-1} - \mu_s\|^2) + C
\end{aligned} \tag{11}$$

where  $C = \frac{1}{2}d + \mathcal{H}(\mathcal{N}(x|\hat{u}_{t-1}, \hat{\Sigma}_{t-1})) - \mathcal{H}(p(\hat{x}_{t-1}|\hat{x}_t)) - \frac{1}{2}\log(\frac{1}{|\hat{\Sigma}_{t-1}|})$  and  $d$  is the dimension of  $x_0$ . Denoted  $\mu_{t-1}$  as the ground truth of the mean of the distribution of  $q(x_{t-1})$  and according to Equation 2, we have  $\mu_{t-1} = \sqrt{\bar{\alpha}_{t-1}}x_0$ .  $\hat{u}_{t-1}$  can be rewritten as :

$$\hat{u} = \mu_{t-1} + e = \sqrt{\alpha_{t-1}}x_0 + e \tag{12}$$

Here,  $e$  is the network prediction error. Since  $\mu_s = \sqrt{\bar{\alpha}_s}x_0$ , Equation 11 can be rewritten as:

$$\begin{aligned}
& \mathcal{D}_{KL}(p(\hat{x}_{t-1}|\hat{x}_t)||q(x_s|x_0)) \\
&= \frac{1}{2}(d\log(1-\bar{\alpha}_s) + \frac{d}{1-\bar{\alpha}_s}\text{Tr}(\hat{\Sigma}_{t-1}) + \frac{1}{1-\bar{\alpha}_s}\|(\sqrt{\alpha_{t-1}} - \sqrt{\alpha_s})x_0 + e\|^2) + C
\end{aligned} \tag{13}$$

if  $s$  is close to  $t-1$ , then  $\sqrt{\alpha_{t-1}} - \sqrt{\alpha_s} \approx 0$ . We have

$$\mathcal{D}_{KL}(p(\hat{x}_{t-1}|\hat{x}_t)||q(x_s|x_0)) \approx \frac{1}{2}(d\log(1-\bar{\alpha}_s) + \frac{d}{1-\bar{\alpha}_s}\text{Tr}(\hat{\Sigma}_{t-1}) + \frac{1}{1-\bar{\alpha}_s}\|e\|^2) + C \tag{14}$$

We further calculate the derivative of  $D_{KL}$  with respect to  $\Sigma_s = 1 - \bar{\alpha}_s$ . We know that  $D_{KL}$  gets its minimum at

$$\Sigma_s = \text{Tr}(\hat{\Sigma}_{t-1}) + \frac{1}{d}\|e\|^2 \tag{15}$$

We next estimate the  $\hat{\Sigma}_{t-1}$  in Equation 15. Assuming each pixel of image  $P \in R^{w \times h}$  follows distribution  $\mathcal{N}(u_i, \sigma)$  with  $\sigma$  being the variance, and  $p_i \perp p_j$  if  $i \neq j$ , then the covariance of  $P$  is  $\sigma\mathbf{I}$

and we have:

$$\begin{aligned}
\sigma_{t-1} &= \frac{(\sum_i (p_i - \bar{p})^2)}{d-1} \\
&= \frac{\sum_i (p_i^2 + \bar{p}^2 - 2p_i\bar{p})}{d-1} \\
&= \frac{\sum_i (p_i^2) - d\bar{p}^2}{d-1}
\end{aligned} \tag{16}$$

Taking expectation on both sides, we achieve

$$\begin{aligned}
\mathbb{E}[\sigma_{t-1}] &= \frac{\sum_i (\mathbb{E}[p_i^2]) - d\mathbb{E}[\bar{p}^2]}{d-1} \\
&= \frac{\sum_i (\sigma + \mu_i^2)}{d-1} - \frac{d}{d-1} \mathbb{E}[(\frac{\sum_i p_i}{d})^2] \\
&= \frac{d\sigma}{d-1} + \frac{\sum_i \mu_i^2}{d-1} - \frac{d}{d-1} \mathbb{E}[(\frac{\sum_i p_i}{d})^2]
\end{aligned} \tag{17}$$

The last term on the RHS of Equation 17 can be rewritten as

$$\begin{aligned}
\frac{d}{d-1} \mathbb{E}[(\frac{\sum_i p_i}{d})^2] &= \frac{d}{d-1} \frac{1}{d^2} (\sum_i \mathbb{E}(p_i)^2 + 2 \sum_{i \neq j} \mathbb{E}(p_i)\mathbb{E}(p_j)) \\
&= \frac{d}{d-1} \frac{1}{d^2} (\sum_i ((\mathbb{E}(p_i))^2 + \sigma) + 2 \sum_{i \neq j} \mathbb{E}(p_i)\mathbb{E}(p_j)) \\
&= \frac{\sigma}{d-1} + \frac{1}{d(d-1)} (\sum_i (\mathbb{E}(p_i))^2 + 2 \sum_{i \neq j} \mathbb{E}(p_i)\mathbb{E}(p_j)) \\
&= \frac{\sigma}{d-1} + \frac{1}{d(d-1)} (\sum_i \mu_i)^2
\end{aligned} \tag{18}$$

By combining Equation 17 and Equation 18 and denoting  $\bar{\mu} = \frac{\sum_i \mu_i}{d}$  we have

$$\begin{aligned}
\mathbb{E}[\sigma_{t-1}] &= \frac{d\sigma}{d-1} + \frac{\sum_i \mu_i^2}{d-1} - \frac{\sigma}{d-1} - \frac{(\sum_i \mu_i)^2}{d(d-1)} \\
&= \sigma + \frac{\sum_i \mu_i^2}{d-1} - \frac{(\sum_i \mu_i)^2}{d(d-1)} \\
&= \sigma + \frac{\sum_i (\mu_i^2) - d\bar{\mu}^2}{d-1} \\
&= \sigma + \frac{\sum_i (\mu_i^2 - 2\mu_i\bar{\mu} + \bar{\mu}^2)}{d-1} \\
&= \sigma + \frac{\sum_i (\mu_i - \bar{\mu})^2}{d-1}
\end{aligned} \tag{19}$$

Here  $\bar{\mu}$  is the mean of  $\mu_i$  and  $\mu_i$  is the mean of the distribution of  $\hat{x}_{t-1}$  at time step  $t-1$ . The ground truth  $x_{t-1} \sim \mathcal{N}(\sqrt{\alpha_{t-1}}x_0, (1-\bar{\alpha}_{t-1})\mathbf{I})$ , thus  $u^{gt} = \sqrt{\alpha_{t-1}}x_0$ . In practice, the  $x_0$  is normalized to stay in the range of  $-1$  to  $1$ , and  $\sqrt{\alpha_t}$  is close to zero when  $t$  is large. Define  $\zeta$  as the difference between  $\mu$  and  $\bar{\mu}$  and denote that  $\zeta_i^{gt} = u_i^{gt} - \bar{\mu}^{gt}$  and  $\hat{\zeta}^i = \mu_i - \bar{\mu}$ , then when  $t$  is large we have  $\zeta_i^{gt} \approx 0$ . Considering the network prediction error, we reach

$$\hat{\zeta}^i = \zeta_i^{gt} + e_i \approx e_i \tag{20}$$

Thus Equation 19 can be rewritten as

$$\mathbb{E}[\sigma_{t-1}] = \sigma + \frac{\sum_i (e_i)^2}{d-1} = \sigma + \frac{\|e\|^2}{d-1} \tag{21}$$

Multiplying  $\mathbb{I}$  on both sides and taking trace

$$d\sigma_{t-1} = d\sigma + \frac{d\|e\|^2}{d-1} \tag{22}$$

Bring Equation 22 to Equation 15

$$\Sigma_s = \sigma_{t-1} - \frac{\|e\|^2}{d(d-1)} \quad (23)$$

In the above derivation, we assume that when  $t$  is large we can reach Equation 23. This assumption corresponds to the cutoff mechanism in our proposed algorithm, where we stop conducting time shift when  $t$  is small, as the assumption does not hold and we are not able to estimate the  $\hat{\Sigma}_{\hat{x}_{t-1}}$  in Equation 15.

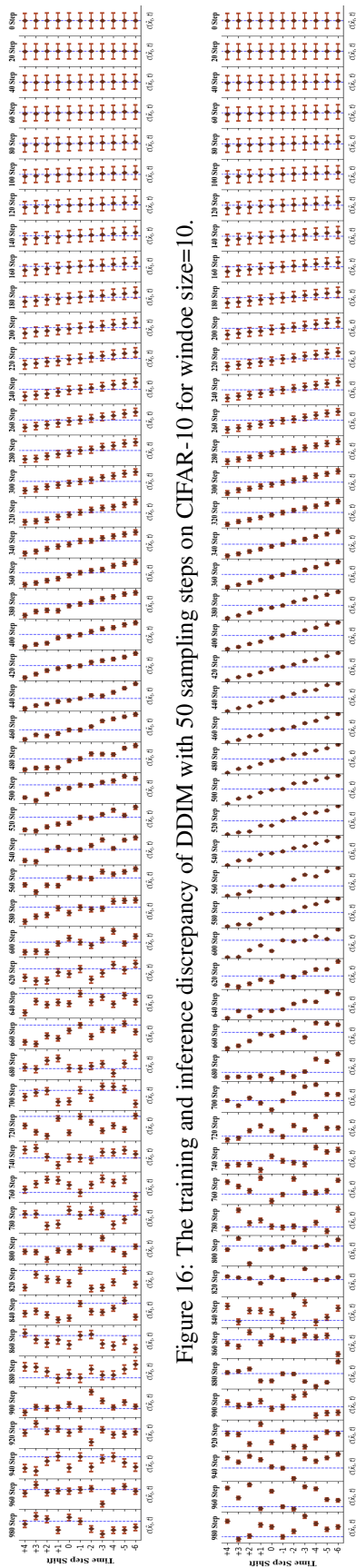


Figure 16: The training and inference discrepancy of DDIM with 50 sampling steps on CIFAR-10 for window size=10.

Figure 17: The training and inference discrepancy of DDIM with 50 sampling steps on CelebA for window size=10.